THE JOURNAL OF PHYSICAL CHEMISTRY B

ARTICLE

pubs.acs.org/JPCB

Merged- and Separate-Band Behavior of the C═O Stretching Band in *N,N*-Dimethylformamide Isotopic Liquid Mixtures: DMF/DMF-d_1, DMF/DMF-d_6, and DMF/DMF-^{13}C═O

Hajime Torii,*,† Maria Grazia Giorgini,*,‡ and Maurizio Musso§

†Department of Chemistry, School of Education, Shizuoka University, 836 Ohya, Shizuoka 422-8529, Japan

‡Dipartimento di Chimica Fisica ed Inorganica, Università di Bologna, Viale del Risorgimento 4, I-40136 Bologna, Italy

§Fachbereich Materialforschung und Physik, Abteilung Physik und Biophysik, Universität Salzburg, Hellbrunnerstrasse 34, A-5020 Salzburg, Austria

ABSTRACT: A combined experimental and theoretical analysis is carried out on the polarized (isotropic and anisotropic) Raman spectra in the spectral region of the C═O stretching (amide I) band of three isotopic liquid mixtures of *N,N*-dimethylformamide (normal/d_1, normal/d_6, and normal/^{13}C═O). Two distinct types of spectral behavior are found for the isotropic Raman spectra: the separate-band behavior (for normal/^{13}C═O), where two separate bands (one for each species) appear at all concentrations but with significant intensity bias, and the merged-band behavior (for normal/d_6), where only one band appears at a frequency between those of the two species and with a band shape noticeably different from the simple overlap of their profiles. An intermediate case between these two limits is also found (for normal/d_1). These main spectral features, as well as the noncoincidence effect (NCE) observed for all the mixtures and neat liquids, are well reproduced by the calculations, meaning that (1) the computational procedure (carried out in the time domain) incorporates all the important factors that determine the main spectral features, and (2) the band merger and the intensity bias are both controlled by the same type of term (resonant intermolecular vibrational coupling) of the vibrational Hamiltonian that gives rise to the NCE. Based on this result, the one- and two-dimensional infrared spectra of the normal/d_1 1:1 mixture are calculated as theoretical predictions. For this purpose, an eigenstate-free method is developed to increase the efficiency of the time-domain spectral calculations and to do the calculations on a largest possible system. The calculated spectral features are compared with those of the polarized Raman spectra and discussed.

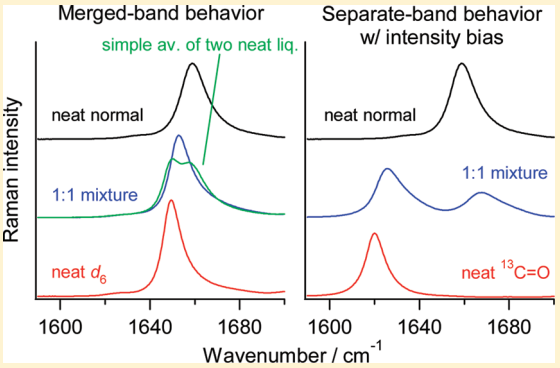

1. INTRODUCTION

Resonant intermolecular vibrational coupling is now well recognized as giving rise to interesting spectroscopic phenomena in the frequency domain and in the time domain.[1] Vibrational modes with large dipole derivatives tend to be strongly coupled because of the transition dipole coupling (TDC).[2−5] Those modes include the OH stretching mode of liquid water[6−14] and alcohols,[15−18] the C═O stretching modes of liquid acetone and other carbonyl compounds,[3,19−27] and the amide I mode of the peptide group[4,5,28−42] in proteins, to name a few. In many cases, particularly in the cases of liquid systems, the vibrational coupling manifests itself in the frequency domain as the noncoincidence effect (NCE),[43,44] a phenomenon that the isotropic and anisotropic Raman bands (and also the infrared (IR) band in some cases) of the same vibrational mode appear at different frequency positions. For the OH stretching mode of liquid water, the coupling gives rise also to a fast decay of the transient IR absorption anisotropy in the time domain.[10,45−50]

The C═O stretching (amide I) mode of liquid formamide is among those vibrational modes with strong intermolecular vibrational coupling. In this particular case, in addition to the NCE, one can also observe another interesting spectroscopic phenomenon: for the 1:1 isotopic liquid mixture of formamide-d_2 ($HCOND_2$) and -d_3 ($DCOND_2$), the isotropic Raman band appears as a merged single band at a frequency position between those of the neat liquids of the two species.[51] This was first interpreted as arising from a mechanism called "mutual entrainment",[51] but in a later theoretical study it was explained by the intermolecular vibrational coupling according to the TDC mechanism,[52] the same mechanism that gives rise to the NCE.

In relation to this spectroscopic phenomenon, there are a few questions to be addressed. (1) Are there any other systems that show the same or similar spectroscopic phenomenon? The previous theoretical study[52] suggested its generality, but experimental confirmation is still lacking. (2) In the case where two separate bands appear (1:1 isotopic liquid mixture of formamide normal species and formamide-^{13}C═O), the theoretical study[52] predicted the occurrence of intensity bias between the two bands

Received: September 21, 2011
Revised: November 8, 2011
Published: November 17, 2011

in the isotropic Raman spectrum. In the observed spectrum, however, it was obscured by the presence of the NH_2 bending band on the low-frequency side.[51] Then, is this intensity bias really an observable spectroscopic phenomenon? An experimental confirmation, with the use of a liquid system free from strong overlapping bands, will be desirable. (3) How is it related to the spectral features of the IR spectra, especially the two-dimensional (2D-) IR[53−61] spectra? It is already well-known that, for neat liquids with a large magnitude of the NCE, the vibrational modes (of a whole liquid system) with strong isotropic Raman intensities are different from those with strong IR intensities. The difference (if any) in the spectral profiles between these spectra of the liquid mixtures should be clarified.

For these purposes, in the present study, a combined experimental and theoretical analysis is carried out on the C═O stretching (amide I) band of liquid *N*,*N*-dimethylformamide (DMF), in which the NH_2 group of formamide is substituted by the $N(CH_3)_2$ group and, hence, there is no self-associative hydrogen-bonding ability and also there is no NH_2 bending vibrational mode. The polarized (isotropic and anisotropic) Raman spectra are measured for three types of isotopic liquid mixtures (normal/d_1, normal/d_6, and normal/^{13}C═O) with mole fractions of x_{normal} = 1.00, 0.75, 0.50, 0.25, and 0.00, and are analyzed with the help of theoretical calculations employing the time-domain computational method developed previously.[10,26,35,36,59−62] It is clearly shown that the merged-band behavior is seen for the isotropic Raman spectra of the normal/d_6 mixtures. In the case where the separate-band behavior is seen (normal/^{13}C═O mixtures), the occurrence of a significant intensity bias in the isotropic Raman spectra is clearly demonstrated. After confirming that the computational procedure incorporates all the important factors that determine the main spectral features of the polarized Raman spectra, the 1D- and 2D-IR spectra of the normal/d_1 1:1 mixture are calculated as theoretical predictions, and their spectral profiles are discussed by comparing them with those of the polarized Raman spectra. An eigenstate-free method is also developed to increase the efficiency of the time-domain calculations of 2D-IR spectra.

2. EXPERIMENTAL METHODS

A. Materials. The normal and d_1 species of DMF [$HCON(CH_3)_2$ and $DCON(CH_3)_2$] were Aldrich products, and the d_6 and ^{13}C═O species [$HCON(CD_3)_2$ and $H^{13}CON(CH_3)_2$] were Isotec (Aldrich) products. All these samples were used without further purification. The normal/d_1, normal/d_6, and normal/^{13}C═O binary liquid mixtures were prepared with mole fractions of x_{normal} = 0.75, 0.50, and 0.25.

B. Spectroscopic measurements. The C═O stretching band of the four isotopic species of DMF (normal, d_1, d_6, and ^{13}C═O) were observed in the spectral region of 1620−1660 cm^{-1} in the liquid state. We obtained the Raman spectra of these neat liquids and of the binary mixtures mentioned above (normal/d_1, normal/d_6, and normal/^{13}C═O) in this spectral region by exciting the samples with the 514.53 nm line emitted by an Ar ion laser (Coherent Innova 300) with a power held constant at 300 mW, by analyzing the Raman scattered light with a spectrometer (Spex 1404) and a multichannel detector (Spex LN2-cooled CCD camera with 1024 × 256 pixels) held at 140 K. The polarization measurements, performed in the 90° scattering geometry configuration, were carried out in the VV and VH polarization configurations by vertically (V) polarizing the exciting laser light and by alternatively selecting the vertically (V) and horizontally (H) polarized components of the Raman scattered light with the use of a polarization sheet. Any parasitic horizontal component in the exciting laser light was eliminated with a Glan-Laser polarizer placed in front of the sample. To compensate for the polarization dependent reflectance of the gratings, the VV and VH polarized Raman scattered light was depolarized by a polarization scrambler placed behind the polarization sheet, before being focused on the entrance slit (width 100 μm, height 10 mm) of the spectrometer. The effective polarization conditions were checked by measuring the depolarization ratio of the depolarized band at 314 cm^{-1} and of the totally polarized band at 459 cm^{-1} of liquid CCl_4, found with values of 0.75 and 0.002, respectively. For the frequency calibration of the spectra, the collection of each VV and VH sample spectrum was followed by that of the corresponding spectrum of a neon calibration lamp. The Ne atomic line at 17 678.28 cm^{-1} was adopted as calibration reference. The Raman measurements were performed at room temperature (293 K) and atmospheric pressure. In the spectroscopic region of interest for this study (around 1640 cm^{-1}), the instrumental slit function amounts to 1.4 cm^{-1}, the detector pixel separation to 0.35 cm^{-1}, and the frequency coverage of the CCD active area to 220 cm^{-1}, thus enabling the simultaneous collection of the C═O stretching bands of both isotopic species present in each mixture. Approximately the same integration time (20 s) and the same accumulation number (20) were used for all isotopic mixtures at different concentrations. The spectral intensity of each mixture was constantly checked against that of the neat liquid normal species and, whenever necessary, the integration time was slightly varied to recover the same initial intensity condition of the latter.

C. Data Treatment and Fitting Strategy. The raw experimental Raman spectra of the C═O stretching spectral region of all neat liquids and isotopic mixtures were analyzed by using the spectroscopy software GRAMS/386. After correction for the frequency drift and CCD response, the VV and VH spectra were combined to obtain the isotropic Raman profiles ($I_{iso} = I_{VV} - 4/3I_{VH}$), the anisotropic ones being directly given by the VH spectra ($I_{aniso} = I_{VH}$).

As indicated in Figure 1, the isotropic Raman spectra of the neat liquids were analyzed by means of four (a−d in Figure 1, for the normal and ^{13}C═O species), five (a−e, for d_6), or six (a−f, for d_1) Gaussian/Lorentzian components. In all cases, two closely located components, a and b in Figure 1, reproduce the blue-side asymmetric band of C═O stretching, one component (c in Figure 1) reproduces the highest frequency band of the spectrum (assigned to the overtone state $2\nu_{16}$ in the case of the normal and ^{13}C═O species, where ν_{16} is the N−CH_3 stretching mode[63]), and one component (d in Figure 1) reproduces the lowest frequency band, assigned, in the cases of the normal and d_6 species and partly also in the case of the d_1 species, to the ^{13}C═O stretching mode of the ^{13}C═O-substituted species present as natural impurity.[64] The same holds for the components of the anisotropic Raman spectra of these neat liquids. The spectral assignment of the intermediate weak bands e (present for d_1 and d_6) and f (present only for d_1) in Figure 1 has not been reported in the literature. As will be commented in section 4, their presence gives rise to some interpretative difficulty.

The isotropic and anisotropic Raman spectra of the binary liquid mixtures were analyzed by means of a variable number (larger than six in most cases) of Gaussian/Lorentzian components depending on their relative intensity and overlap. In the case of the normal/d_6 mixtures, six components were required,

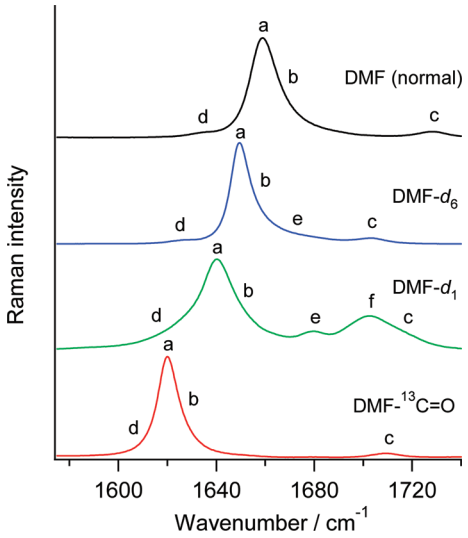

Figure 1. Isotropic Raman spectra of the C═O stretching region in neat liquid DMF normal, d_6, d_1, and ^{13}C═O species. Labels a−f indicate the component bands included in the fitting to reproduce the whole spectrum. a,b: The fundamental C═O stretching band, decreasing in frequency with the increase of the reduced mass of the oscillator, with b being the component mimicking the blue-side asymmetry of this band. c: The highest frequency component, representing in the cases of the normal and ^{13}C═O species an overtone state $2\nu_{16}$, where ν_{16} is the N−CH_3 stretching mode. d: The lowest frequency component, representing in the cases of the normal and d_6 species and partly also in the case of the d_1 species the ^{13}C═O stretching band of the ^{13}C═O substituted species [$H^{13}CON(CH_3)_2$ for the normal species, $H^{13}CON(CD_3)_2$ for the d_6 species, and $D^{13}CON(CH_3)_2$ for the d_1 species] present as natural impurity. e: Additional component present for the d_1 and d_6 species. f: Further additional component present for the d_1 species.

two of which were used for representing the merged asymmetric band of C═O stretching with a frequency in the range between those of the two constituent neat liquids, while the remaining two c's and two d's persisted at approximately the same frequencies of those of the two neat liquids (see section 4).

The band parameters entered in the fitting procedure were chosen to achieve the best compromise between the χ^2 value of the fitting and the uncertainties of the optimized parameters. The C═O stretching main band is blue-side asymmetric and its first moment was determined as the weighted average of the two component peak frequencies contributing to it.

3. COMPUTATIONAL PROCEDURE

The calculations in the present study were carried out with essentially the same method as in our previous studies on the 1D and 2D vibrational spectra of neat liquid DMF normal species,[59−61] except for the parametrization for the isotopic species and the newly adopted piece of method described in section 3D. However, for completeness of the paper, the whole computational procedure is briefly described below. This is based on a hierarchical combination of two techniques,[10,26,34−36,48−50,59−62] classical molecular dynamics (MD) simulations on the time-dependent molecular configurations in liquids, and time-domain quantum mechanical calculations of the 1D and 2D vibrational spectra of a particular vibrational band (the C═O stretching band in the present case).

A. Classical MD Simulations. The MD simulations were performed with a five-site model of DMF, where the CH and CH_3 groups were treated as united atoms. The partial charges on these five sites were determined by fitting to the electrostatic potential around an isolated DMF molecule,[59−61] and the Lennard-Jones parameters were taken from ref 65. The total number of molecules N was set to 128 for calculating the 1D-IR and Raman spectra, but it was inevitable to reduce it to 64 for calculating the 2D-IR spectra because of the much higher demand of computational power (see also section 3D). As in the experiments, the cases of the following three types of isotopic mixtures were studied: normal/d_1, normal/d_6, and normal/^{13}C═O. The mole fractions were set to x_{normal} = 1.0, 0.75, 0.5, 0.25, and 0.0. The size of the cubic simulation cell was fixed by referring to the molecular volume v_{mol} = 127.9 Å^3, and the temperature was kept to T = 293 K. The time step was set to 2 fs. The total lengths of the simulations were determined from the spectral resolution (obtained after the Fourier transformation) and the number of samples for spectral averaging, which are described below in section 3C.

B. Construction of the Vibrational Hamiltonians. On the basis of the time-dependent molecular configurations in liquids, the vibrational Hamiltonians of the one- and two-quantum excited states (whose dimensions are N and $N(N + 1)/2$, respectively, and denoted as H^{1Q} and H^{2Q} hereafter) of the C═O stretching mode were constructed as follows. The modulations in the diagonal terms of H^{1Q} due to the effects of the electric fields from the surrounding molecules[66−72] are expressed as[10,35,36,59−61]

$$\Delta H^{1Q}_{mm} = \frac{\hbar}{2\sqrt{k_m}}\left(\frac{f_m}{k_m}\frac{\partial \boldsymbol{\mu}_m}{\partial q_m} - \frac{\partial^2 \boldsymbol{\mu}_m}{\partial q_m^2}\right)\mathbf{E}_m \qquad (1)$$

where k_m and f_m are the diagonal quadratic and cubic mass-weighted force constants for the C═O stretching vibration of the mth molecule (q_m), $\partial \boldsymbol{\mu}_m/\partial q_m$ and $\partial^2 \boldsymbol{\mu}_m/\partial {q_m}^2$ are the dipole first and second derivatives of this vibration, and $\boldsymbol{E}_m$ is the electric field operating on the mth molecule. This equation describes the shift of H^{1Q}_{mm} from $\hbar(k_m)^{1/2}$, which corresponds to the vibrational frequency of an isolated DMF molecule. The modulations in the diagonal terms of H^{2Q} are given as

$$\Delta H^{2Q}_{m+n,m+n} = \Delta H^{1Q}_{mm} + \Delta H^{1Q}_{nn} - \delta_{mn}\frac{5\hbar^2}{24}\left(\frac{f_m}{k_m}\right)^2 \qquad (2)$$

where "m+n" in the subscript stands for the state with one quantum each on the mth and nth molecules ($m \neq n$) or with two quanta on the mth molecule ($m = n$). The third term is effective only for the latter type of states and represents the effect of mechanical anharmonicity on the energy levels of the two-quantum excited states.

The value of k_m of the normal species (= 6.1060 × 10^{-5} E_h ${a_0}^{-2}$ ${m_e}^{-1}$ or 1.7329 mdyn Å^{-1} amu^{-1}) was obtained[59−61] from the observed vibrational frequency in the gas phase,[63,73] and those of the other isotopic species (k_m = 5.9795, 6.0500, and 5.8144 × 10^{-5} E_h ${a_0}^{-2}$ ${m_e}^{-1}$ or 1.6970, 1.7170, and 1.6502 mdyn Å^{-1} amu^{-1} for the d_1, d_6, and ^{13}C═O species, respectively) were determined by referring to their ratios calculated at the MP3/6-31+G(2d,p) level by using the Gaussian 03 program.[74] The values of f_m/k_m, the magnitudes and directions of $\partial \boldsymbol{\mu}_m/\partial q_m$ and $\partial^2 \boldsymbol{\mu}_m/\partial {q_m}^2$, as well as the direction of the principal axis of the $\partial \boldsymbol{\alpha}_m/\partial q_m$ tensor (assumed axially symmetric), were also determined by referring to the values calculated at the MP3/6-31+G(2d,p)

dx.doi.org/10.1021/jp209119e |J. Phys. Chem. B 2012, 116, 353–366

Table 1. Values of the Parameters Used for Constructing the Vibrational Hamiltonians for the C═O Stretching Modes of DMF Isotopic Species

parameter	normal	d_1	d_6	^{13}C═O
$k_m/10^{-5}\ E_h\ a_0^{-2}\ m_e^{-1}$	6.1060	5.9795	6.0500	5.8144
$(f_m/k_m)/10^{-2}\ a_0^{-1}\ m_e^{-1/2}$	−2.11	−2.05	−2.43	−2.18
$\lvert\partial\boldsymbol{\mu}_m/\partial q_m\rvert/10^{-2}\ e\ m_e^{-1/2}$	1.5407	1.5849	1.5568	1.4925
$\partial\boldsymbol{\mu}_m/\partial q_m$, angle[a]/deg.	24.1	26.9	24.0	23.8
$\lvert\partial^2\boldsymbol{\mu}_m/\partial q_m^2\rvert/10^{-5}\ e\ a_0^{-1}\ m_e^{-1}$	4.4635	2.9526	4.9476	4.2081
$\partial^2\boldsymbol{\mu}_m/\partial q_m^2$, angle[a]/deg	−172.6	−157.7	−167.7	−175.5
$\partial\boldsymbol{\alpha}_m/\partial q_m$, principal axis, angle[a]/deg	29.8	28.1	29.6	30.0

[a] Angle from the $\boldsymbol{r}_{CO}$ ($\equiv\boldsymbol{r}_C - \boldsymbol{r}_O$) direction toward the $\boldsymbol{r}_{NC}$ direction.

level (with scaling[59,60] by 0.85 for $\partial\boldsymbol{\mu}_m/\partial q_m$ and $\partial^2\boldsymbol{\mu}_m/\partial q_m^2$). The values of the parameters actually used in the calculations are summarized in Table 1. The interaction point between the dipole first and second derivatives and the electric field in eq 1 was assumed to be located at the center of the C═O bond.

The off-diagonal terms of H^{1Q} were determined by the transition dipole coupling (TDC) mechanism,[2−5,10,26,28−36,48−50,59−62] expressed as

$$H_{mn}^{1Q} = -\frac{\hbar}{2(k_m k_n)^{1/4}}\frac{\partial\boldsymbol{\mu}_m}{\partial q_m}\cdot\mathbf{T}_{mn}\cdot\frac{\partial\boldsymbol{\mu}_n}{\partial q_n} \qquad (m \neq n) \tag{3}$$

where $\mathbf{T}_{mn}$ is the dipole interaction tensor between the mth and nth molecules, which is given as

$$\mathbf{T}_{mn} = \frac{3\mathbf{r}_{mn}\mathbf{r}_{mn} - r_{mn}^2\mathbf{I}}{r_{mn}^5} \tag{4}$$

where $\boldsymbol{r}_{mn} = \boldsymbol{r}_m - \boldsymbol{r}_n$ is the distance vector (of length r_{mn}) between the molecules, and $\mathbf{I}$ is a 3×3 unit tensor. In this case also, the interaction point was assumed to be located at the center of the C═O bond.

The off-diagonal terms of H^{2Q} were evaluated in the harmonic approximation as

$$\frac{1}{\sqrt{2}}H_{l+m,m+m}^{2Q} = H_{l+n,m+n}^{2Q} = H_{lm}^{1Q} \quad (l \neq m,\ l \neq n, m \neq n) \tag{5}$$

This form is obtained because of the bilinear nature, which allows only an excitation and a de-excitation by one quantum each (on the lth and mth molecules in eq 5), of the coupling Hamiltonian according to the TDC mechanism evaluated in the harmonic approximation. As a result, there are many zero elements in H^{2Q}; for example, $H_{m+m,n+n}^{2Q} = 0$ if $m \neq n$, while H_{mn}^{1Q} is generally nonzero. This gives rise to the sparse nature of H^{2Q} (for a sufficiently large value of N), with only at most $2N - 1$ nonzero elements (among the $N(N+1)/2$ elements in total) on each row or column. This sparse nature is utilized in the method of time evolution described in section 3D.

C. Calculations of the 1D and 2D Spectra. By use of the vibrational Hamiltonians H^{1Q} and H^{2Q} thus constructed, the 1D and 2D vibrational spectra were calculated with a time-domain method.[10,26,34−36,48−50,59−62] The 1D polarized Raman spectrum is expressed as

$$I_{pq}^{(R)}(\omega) = \mathrm{Re}\int_0^\infty \mathrm{d}t\,\exp(i\omega t - \gamma t)\left\langle\langle 0|\alpha_{pq}(t)|\psi_{pq}^{(R)}(t,0)\rangle\right\rangle \tag{6}$$

where $\alpha_{pq}(t)$ is the pq element (where $p, q = 1, 2, 3$ corresponds to the x, y, and z axes of the system) of the polarizability operator $\boldsymbol{\alpha}$ ($\equiv\Sigma_m\boldsymbol{\alpha}_m$) at time t, $|\psi_{pq}^{(R)}(t,t_0)\rangle$ (with $t_0 = 0$ in this equation) is the wave function of the one-quantum Raman excitations at time t (described below), γ is an empirical parameter for the vibrational population relaxation, and the large bracket stands for statistical average. The 1D-IR spectrum is similarly calculated, by replacing the polarizability operator by the dipole operator.[10,26,35,36,59−62] The value of γ was assumed to be 0.47 ps^{-1} from the comparison between the observed[75] and calculated isotropic Raman band widths of neat liquid DMF normal species (i.e., to compensate for the difference between these in the previous study[60]). Note that, because this γ is used commonly to all kinds of spectra, we can discuss, for example, the difference in the band widths between the isotropic and anisotropic Raman spectra.

The time evolutions of $|\psi_{pq}^{(R)}(t,t_0)\rangle$, which is an N-dimensional vector, were calculated by using $H^{1Q}(t)$ as

$$|\psi_{pq}^{(R)}(t,t_0)\rangle = \exp_+\left[-\frac{i}{\hbar}\int_{t_0}^{t}\mathrm{d}\tau\,H^{1Q}(\tau)\right]|\psi_{pq}^{(R)}(t_0,t_0)\rangle \tag{7}$$

where $\exp_+$ denotes the time-ordered exponential. This time-ordered exponential was evaluated as a product of the time evolutions during short times $\Delta\tau$ (taken as equal to the MD time step, 2 fs) as[10,26,34−36,48−50,59−62]

$$|\psi_{pq}^{(R)}(\tau + \Delta\tau, t_0)\rangle = \exp[-i\Delta\tau H^{1Q}(\tau)/\hbar]|\psi_{pq}^{(R)}(\tau,t_0)\rangle \tag{8}$$

assuming that $H^{1Q}(\tau)$ is essentially invariant during $\Delta\tau$. The total duration of the time evolutions was set to ∼65.5 ps (32 768 steps) to obtain a frequency resolution of ∼0.5 cm^{-1}. The initial wave functions were spawned with an interval of ∼32.8 ps, and the statistical average in eq 6 was taken over 450 samples (1350 samples for neat normal species).

The 2D-IR spectra, with the waiting time between the second and third pulses being set to zero, were calculated also in the time domain on the basis of the diagrams shown in Figure 1 of ref 60. The spectra of both the rephasing and nonrephasing optical processes as well as their sum (the absorptive spectrum) were calculated, with the polarizations of the pulses being assumed as all parallel (the *zzzz* polarization) or as perpendicular (the *xxzz* polarization). The explicit formulas of the spectra were shown in ref 60. The time evolutions of the wave functions were calculated with the same value of $\Delta\tau$ (=2 fs) as the case of the 1D spectra, and the total duration of the time evolutions (the sum of those for the two frequency axes of the 2D-IR spectra) was set to ∼32.8 ps (16 384 steps) to obtain a frequency resolution of ∼2 cm^{-1}. The initial wave functions were spawned with an interval of ∼2 ps. The 2D-IR spectra were smoothed with a Gaussian function with the fwhm of 8 cm^{-1}, and the statistical average was taken over 245 samples.

D. Eigenstate-Free Method of Time Evolution. In the computations of 2D-IR spectra with the time-domain formulas, the most time-consuming part is the time evolution of the two-quantum excited vibrational states according to

$$|\psi^{2Q}(\tau + \Delta\tau)\rangle = \exp[-i\Delta\tau H^{2Q}(\tau)/\hbar]|\psi^{2Q}(\tau)\rangle \tag{9}$$

where $|\psi^{2Q}(\tau)\rangle$ generally stands for a two-quantum excited vibrational state, because of its large dimension [$=N(N+1)/2$]. Since it scales as $\sim N^2$, the problem is more serious for larger

systems. Meanwhile, since the present study deals with liquid mixtures, it is preferable to carry out calculations on a largest possible system. In our previous calculations of 2D-IR spectra, the system size was limited to $N = 32$,[59−61] and $H^{2Q}(\tau)$ was diagonalized every time step (with the interval of $\Delta\tau$) for the time evolution of $|\psi^{2Q}(\tau)\rangle$.[36,59−61] Here we propose an eigenstate-free method as described in the following.

We take an approximate center angular frequency ω_c^{2Q} of the two-quantum excited vibrational states, and decompose $\exp[-i\Delta\tau H^{2Q}(\tau)/\hbar]$ as

$$\exp[-i\Delta\tau H^{2Q}(\tau)/\hbar] = \exp(-i\Delta\tau\omega_c^{2Q}I) \times \exp[-i\Delta\tau(H^{2Q}(\tau)/\hbar - \omega_c^{2Q}I)] \quad (10)$$

where I is the unit matrix of size $N(N+1)/2$. Then, the latter factor is expanded and truncated at the mth order term as

$$\exp[-i\Delta\tau(H^{2Q}(\tau)/\hbar - \omega_c^{2Q}I)] \cong \sum_{k=0}^{m}\frac{1}{k!}[-i\Delta\tau(H^{2Q}(\tau)/\hbar - \omega_c^{2Q}I)]^k \quad (11)$$

This is a matrix of size $N(N+1)/2$, and it is possible to operate it directly to $|\psi^{2Q}(\tau)\rangle$ ($N(N+1)/2$-dimensional vectors). It is possible to fully utilize the sparse nature of $H^{2Q}(\tau)$ in calculating $(H^{2Q}(\tau)/\hbar - \omega_c^{2Q}I)^k$ up to $k = m$. The error arising from the truncation is determined by m, $\Delta\tau$, and the largest magnitude of the eigenvalues of $H^{2Q}(\tau)/\hbar - \omega_c^{2Q}I$, and is estimated as follows. For a real number x (intended to be equal to the product of $\Delta\tau$ and the largest magnitude of the eigenvalues of $H^{2Q}(\tau)/\hbar - \omega_c^{2Q}I$), we have

$$\left|\exp(-ix) - \sum_{k=0}^{m}\frac{1}{k!}(-ix)^k\right| = \left|\sum_{k=m+1}^{\infty}\frac{1}{k!}(-ix)^k\right| \le \sum_{k=m+1}^{\infty}\frac{1}{k!}|x|^k \equiv D(x;m) \quad (12)$$

The values of $D(x;m)$ are plotted against m for a few fixed values of x in Figure 2. It is seen that, e.g., for $x = 0.3$, $D(x;m)$ is as small as $\sim 10^{-13}$ at $m = 10$. The value $x = 0.3$ corresponds to $\Delta\tau = 2$ fs and the coverage of the frequency range of ± 796 cm^{-1}, which is considered to be sufficiently wide for the first overtone region of the C═O stretching mode of DMF. We therefore adopt truncation at $m = 10$ in the present calculations. It is also noticed from Figure 2 that a reduction of $\Delta\tau$ by a factor of 3, for example, leads to only a modest decrease in the order of truncation ($m = 7$) to obtain the same level of accuracy with the coverage of the same frequency range. Therefore, generally speaking, retaining up to a sufficiently high order term rather than reducing the time interval $\Delta\tau$ is efficient for calculations with a minimal truncation error, as long as $H^{2Q}(\tau)$ is safely treated as invariant during $\Delta\tau$ (which is a basic assumption for eq 9).

With this time evolution scheme, the computational time needed for calculating 2D-IR spectra (averaged over 245 samples, for one isotopic composition) was equivalent to ~269 h (for rephasing) and ~890 h (for nonrephasing) on a Dell PowerEdge 2950 server with dual Xeon 5160 processors (4 cores in total). It is expected to scale as $\sim N^5$, taking into account the number of elements ($\sim N^4$) of $(H^{2Q}(\tau)/\hbar - \omega_c^{2Q}I)^k$ and the sparse nature of $H^{2Q}(\tau)$ (at most $2N-1$ nonzero elements on each row or column) utilized in calculating them.

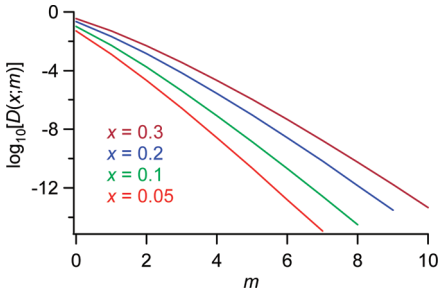

Figure 2. Values of $\log_{10}[D(x;m)]$ defined by eq 12 plotted against m for $x = 0.05$, 0.1, 0.2, and 0.3.

4. RESULTS AND DISCUSSION

A. Observed and Calculated Polarized Raman Spectra. The observed and calculated isotropic and anisotropic Raman spectra of the C═O stretching spectral region of the normal/d_1, normal/d_6, and normal/^{13}C═O mixtures are shown in Figures 3, 4, and 5, respectively. In each figure the top-left and bottom-left panels (a and b) show the observed isotropic and anisotropic Raman spectra, respectively, while the top-right and bottom-right panels (c and d) show the isotropic and anisotropic Raman spectra calculated according to eq 6 with the appropriate p,q combinations of $I_{pq}^{(R)}(\omega)$. Within each panel the spectra from top to bottom (stacked for clarity) display the C═O stretching spectral region of the binary mixtures at different mole fractions $x_{normal} = 1.00$, 0.75, 0.50, 0.25, and 0.00.

Frequencies. The C═O stretching bands of the d_1, d_6, and ^{13}C═O species occur, as generally observed in H/D and ^{12}C/^{13}C isotopic substitution, at frequencies lower than that of the normal species due to the increase of the reduced mass.[63] As revealed from the comparison of the spectra at $x_{normal} = 1.00$ and 0.00 in panels a and b (isotropic and anisotropic Raman, respectively) of Figures 3−5, the most remarkable frequency lowering is seen for the ^{13}C═O species (about −40 cm^{-1}, Figure 5), since this ^{13}C atom directly participates in the C═O stretching motion. A less remarkable frequency lowering of about −10 cm^{-1} is seen for the d_6 species (Figure 4), since here the deuterium atoms of the methyl groups only partially participate in the C═O stretching motion. An intermediate frequency lowering of about −20 cm^{-1} is observed for the d_1 species (Figure 3), since the proximity of the deuterium atom to the carbonyl group in this isotopic species allows its more direct participation in the C═O stretching vibration. The same frequency order observed for the C═O stretching band of the neat liquids ($\nu_{normal} > \nu_{d6} > \nu_{d1} > \nu_{13C=O}$) holds as well for the values of the mass-weighted force constant k_m shown in Table 1.

Both the isotropic and anisotropic Raman spectral profiles of the C═O stretching main band are blue-side asymmetric, even though at a different degree in the different isotopic species considered here. This makes the first moments of both the isotropic and anisotropic Raman bands always higher than the corresponding peak frequencies, as seen in Table 2.

As explained also in section 2C, in both the isotropic and anisotropic Raman spectra of the neat normal species, the C═O stretching band is accompanied by a weak band appearing at approximately 1729 cm^{-1}, which is considered to be due to the overtone $2\nu_{16}$.[63] It is worth remarking that its frequency only marginally changes with concentration (panel a in Figures 3−5) and its intensity roughly scales with the mole fraction of the

dx.doi.org/10.1021/jp209119e |J. Phys. Chem. B 2012, 116, 353–366

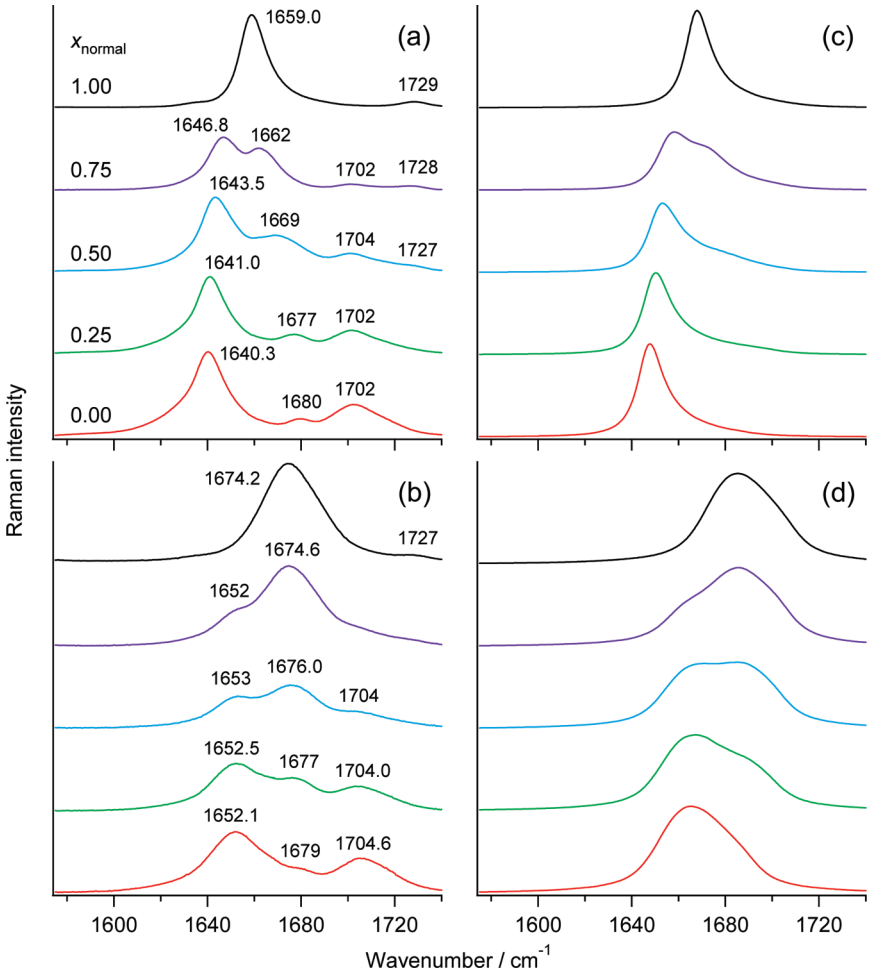

Figure 3. Isotropic (top panels, a and c) and anisotropic (bottom panels, b and d) Raman spectra of the C═O stretching region of liquid DMF normal/d_1 isotopic mixtures. Left (a,b), experimental results; right (c,d), calculated results (eq 6). Observed Raman intensities are not normalized but consistent with each other within each panel, while the isotropic and anisotropic Raman intensities have been scaled by the ratio 1:5.36 to match with the figure frames. The frequencies of some main features in the observed spectra are labeled.

normal species. It could be thought of as a sort of internal intensity standard and, indeed, we have used it as a check of spectral intensity in the mixtures.

We remark the presence of an additional satellite band in the lower frequency side of the C═O stretching main band of neat normal species, at approximately 1635 cm^{-1}, attributable to the ^{13}C═O stretching vibration of the ^{13}C═O species present as natural impurity. Thanks to the observability of this band (component d in Figure 1), we are able to recognize different contributions to the gas-to-liquid frequency downshifts of the isotropic Raman band: the diagonal contribution given by eq 1 arising from the environmental perturbations, and the off-diagonal contribution given by eq 3 arising from the intermolecular vibrational coupling. The first may be obtained from the difference between the ^{13}C═O stretching frequencies of the ^{13}C═O species present as natural impurity in the normal liquid (1635 cm^{-1}) and in the gas phase (1673 cm^{-1}),[63] and amounts to −38 cm^{-1}. The second is obtained from the difference between the ^{13}C═O stretching frequencies of neat liquid ^{13}C═O species (1620.9 cm^{-1}) and the ^{13}C═O species present as natural impurity in the normal liquid (1635 cm^{-1}), and amounts to −14 cm^{-1}. The values of these two quantities evaluated by using eqs 1 and 3 are −33 and −15 cm^{-1}, respectively. Since the gas-to-liquid frequency shifts occurring in all the isotopic species amount to approximately the same value (−56 cm^{-1} for the normal species, −53 cm^{-1} for d_6, and −57 cm^{-1} for d_1), it will be reasonable to consider that they may be partitioned in the same way into the diagonal (environmental) and off-diagonal (intermolecular vibrational coupling) contributions.

Bandwidths. The widths (fwhms) of the C═O stretching main band in the isotropic and anisotropic Raman spectra of all the isotopic species have been evaluated after subtraction of the satellite bands not relevant to the main band. The observed bandwidths amount to 14.0, 14.5, 10.4, and 10.4 cm^{-1} in the isotropic Raman spectra of the neat liquid normal, d_1, d_6, and ^{13}C═O species, respectively. Those in the anisotropic Raman spectra are larger and amount to 29.9, 28.0, 30.9, and 30.4 cm^{-1}, respectively.

Noncoincidence Effect. As shown in panels a and b of Figures 3−5, in the case of the neat liquid normal species, the C═O stretching band appears at 1659.0 cm^{-1} (peak) or 1661.8 cm^{-1} (first moment) in the isotropic Raman spectrum, and at 1674.2 cm^{-1} (peak) or 1677.1 cm^{-1} (first moment) in the anisotropic Raman spectrum, indicating[75,76] the occurrence of a large frequency separation between the anisotropic and isotropic Raman bands ($\nu_{aniso} - \nu_{iso} \approx 15$ cm^{-1}), a phenomenon referred

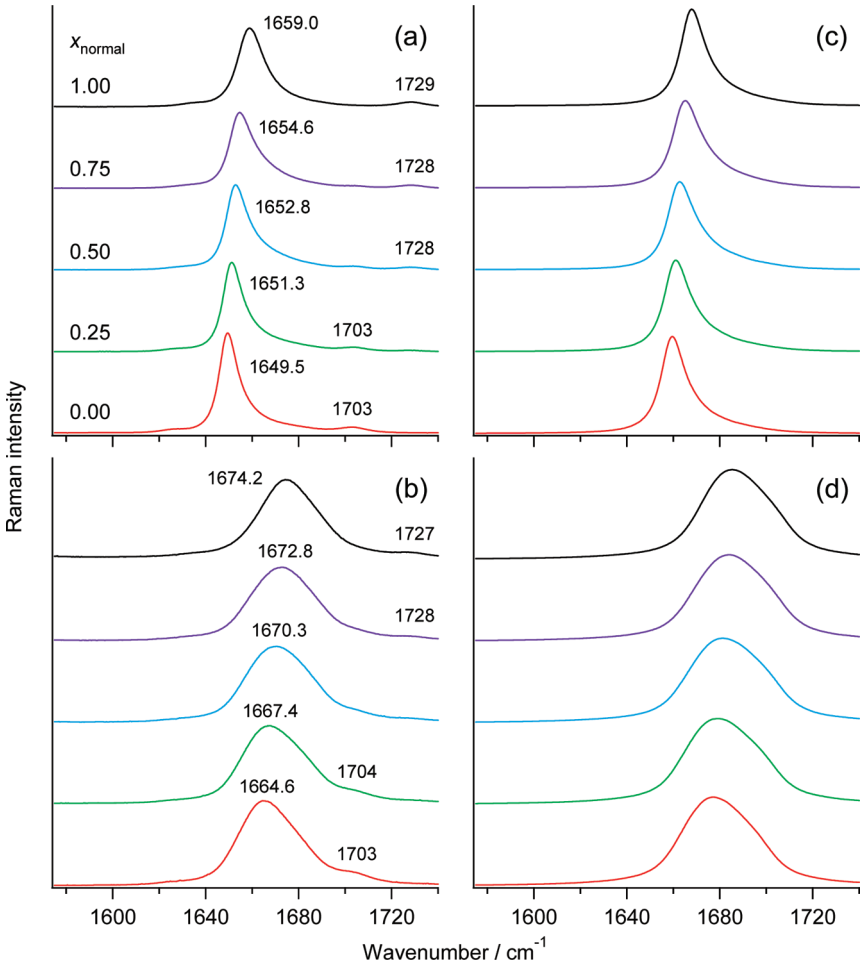

Figure 4. Isotropic (top panels, a and c) and anisotropic (bottom panels, b and d) Raman spectra of the C═O stretching region of liquid DMF normal/d_6 isotopic mixtures. Left (a,b), experimental results; right (c,d), calculated results (eq 6). Observed Raman intensities are not normalized but consistent with each other within each panel, while the isotropic and anisotropic Raman intensities have been scaled by the ratio 1:5 to match with the figure frames. The frequencies of some main features in the observed spectra are labeled.

to as noncoincidence effect (NCE).[43,44] The same phenomenon is seen also for the other isotopic species, but for the d_1 species the NCE amounts to only 10 cm^{-1} (Table 2). Usually, the NCE evaluated from the peak frequencies is larger than that evaluated from the first moments, because the isotropic Raman band is typically blue-side asymmetric in the presence of intermolecular vibrational coupling. However, for all the isotopic species of DMF considered here, the C═O stretching band in the anisotropic Raman spectrum appears to be blue-side asymmetric to an extent comparable to that in the isotropic Raman spectrum. This causes the NCE values evaluated from the peak frequencies to be slightly smaller than those evaluated from the first moments.

It has been widely recognized[1−3,44] that the NCE represents a spectroscopic manifestation of the occurrence of the resonant intermolecular interaction between nearby IR-active oscillators, such as the C═O stretching, through the TDC mechanism. This vibrational coupling induces resonant vibrational energy transfer when a short-range order is created in the liquid structure by dipolar[19−27] or nondipolar[6−18] forces. The blue-side asymmetry of the isotropic Raman bands is a further indication of the occurrence of resonant intermolecular coupling between nearby C═O stretching oscillators.[24,77]

The NCE is related to both the degree of short-range order and to the strength of the intermolecular vibrational coupling. Within the Born−Oppenheimer approximation, the electric dipole moment, and hence the degree of short-range order in dipolar liquids, should stay constant among different isotopic species. By contrast, the variation in the C═O stretching normal coordinate with isotopic substitution alters the value of the dipole derivative $\partial\mu/\partial q$ of this mode, hence producing a variation in the strength of the intermolecular vibrational coupling and, as a consequence, a variation in the NCE among the different isotopic species. According to the change in the dipole derivative shown in Table 1, we should expect NCE variation in the order of $NCE_{d1} > NCE_{d6} > NCE_{normal} > NCE_{13C=O}$. The experimental result, $NCE_{d6} > NCE_{normal} > NCE_{13C=O} > NCE_{d1}$, contradicts this order. We consider that this may be a consequence of the presence of the overtone state at 1679 cm^{-1} of the d_1 species that is possibly in Fermi resonance with the C═O stretching fundamental mode, which can alter both the frequency and the intensity of the C═O stretching band.

Spectral Effects of the Isotopic Dilution. By inspecting the spectra shown in panels a and b of Figures 3−5, we can recognize the occurrence of two distinct types of spectral behavior of the C═O stretching bands upon dilution: one is exhibited by the

dx.doi.org/10.1021/jp209119e |*J. Phys. Chem. B* 2012, 116, 353–366

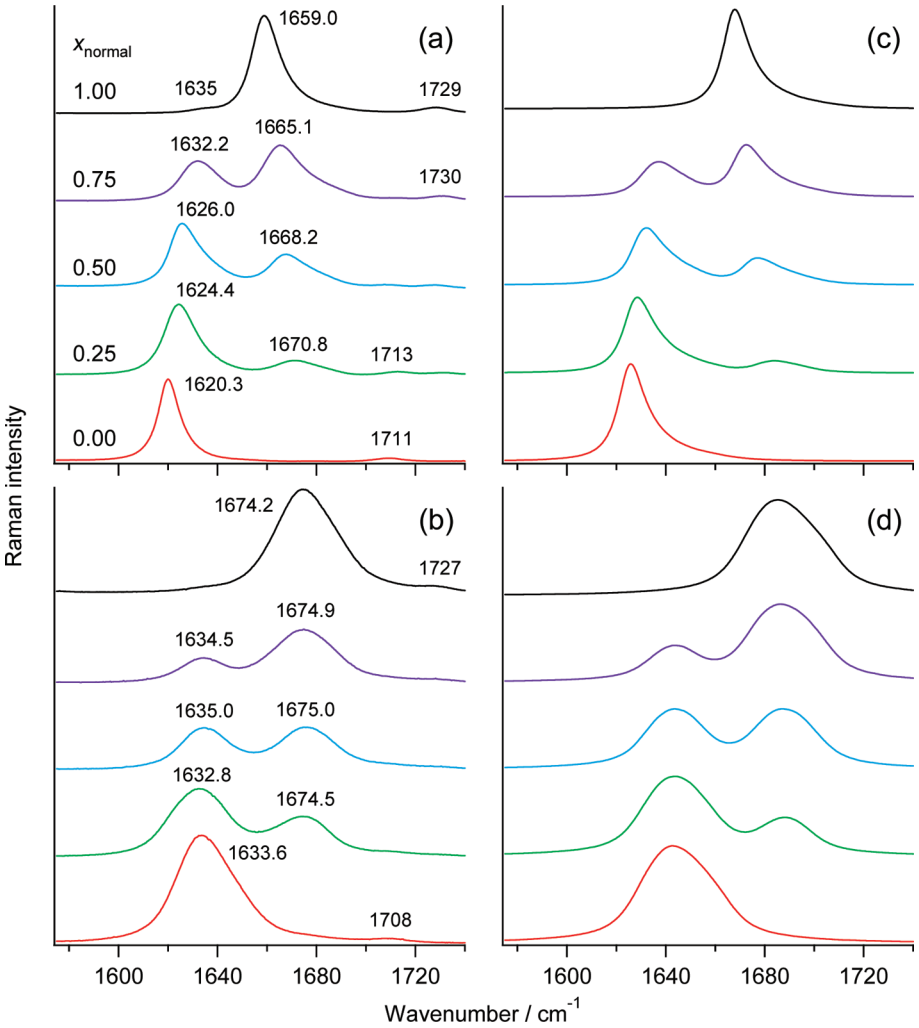

Figure 5. Isotropic (top panels, a and c) and anisotropic (bottom panels, b and d) Raman spectra of the C═O stretching region of liquid DMF normal/^{13}C═O isotopic mixtures. Left (a,b), experimental results; right (c,d) calculated results (eq 6). Observed Raman intensities are not normalized but consistent with each other within each panel, while the isotropic and anisotropic Raman intensities have been scaled by the ratio 1:5.36 to match with the figure frames. The frequencies of some main features in the observed spectra are labeled.

Table 2. Observed First Moments and Peak Frequencies, and the Corresponding NCEs of the C═O Stretching Main Band, in the Isotropic and Anisotropic Raman Spectra of the Neat Liquid DMF Isotopic Species

	first moment			peak frequency		
	iso	aniso	NCE	iso	aniso	NCE
normal	1661.75(2)	1677.11(5)	15.36(8)	1659.0(1)	1674.2(3)	15.2(4)
d_1	1642.7(1)	1652.7(2)	10.0(3)	1640.3(3)	1652.1(4)	11.8(7)
	1639.3(2)[a]	1649.4(4)[a]	10.1(6)[a]			
d_6	1651.09(3)	1668.27(6)	17.18(9)	1649.5(2)	1664.6(2)	15.1(4)
^{13}C═O	1620.88(4)	1634.92(8)	14.0(1)	1620.3(1)	1633.6(2)	13.3(3)

[a] Evaluated by including the band at 1626 cm^{-1}.

normal/^{13}C═O mixtures (Figure 5), and the other is the normal/d_6 mixtures (Figure 4).

In the first case, both the isotropic and anisotropic Raman C═O stretching bands of the normal and ^{13}C═O species preserve their individuality over the whole dilution range, a behavior which can be referred to as "separate-band behavior". Upon dilution (top to bottom) the isotropic Raman band of the normal species increases in frequency from 1659 cm^{-1} (x_{normal} = 1.0) up to approximately 1671 cm^{-1} (x_{normal} = 0.25), and that of the ^{13}C═O species decreases from 1632 cm^{-1} (at x_{normal} = 0.75) [or from 1635 cm^{-1} at x_{normal} = 1.00] to 1620 cm^{-1} in the neat liquid (x_{normal} = 0.00). The frequency upshift of the former (downshift of the latter) is the consequence of the progressive removal (onset) of intermolecular vibrational coupling among the ^{12}C═O (^{13}C═O) stretching oscillators, as verified previously for the C═O stretching band in the liquid acetone normal/^{13}C═O mixtures.[27] As expected from theoretical consideration[2] that the frequency shift of the anisotropic Raman band upon dilution is only 1/25 of that of the isotropic Raman band, the observed frequencies of the anisotropic Raman bands of the two C═O stretching oscillators remain approximately constant at 1674 and 1634 cm^{-1}, respectively. Additionally, as shown in Figure 6a, both the isotropic and anisotropic Raman band frequencies (first moments) of the ^{12}C═O and ^{13}C═O stretching bands manifest linear concentration dependence, as expected[2] for isotopic mixtures. As far as the C═O stretching band intensity

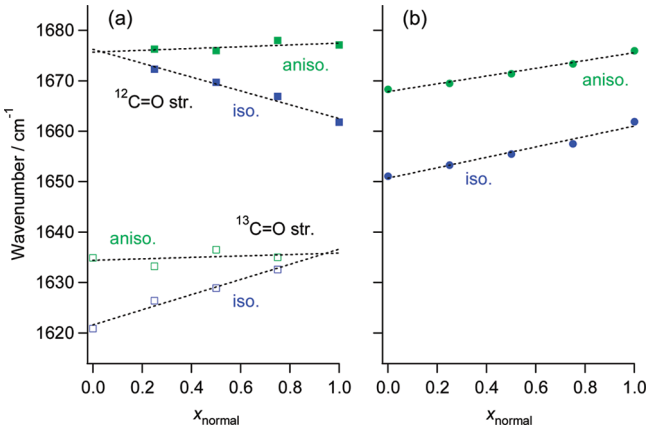

Figure 6. Observed isotropic and anisotropic Raman band position (first moment) shifts of (a) the separate ^{12}C═O and ^{13}C═O stretching of the normal and ^{13}C═O species in liquid DMF normal/^{13}C═O isotopic mixtures, and (b) the merged C═O stretching of the normal and d_6 species in liquid DMF normal/d_6 isotopic mixtures. The dotted lines show the results of the fitting to the observed values.

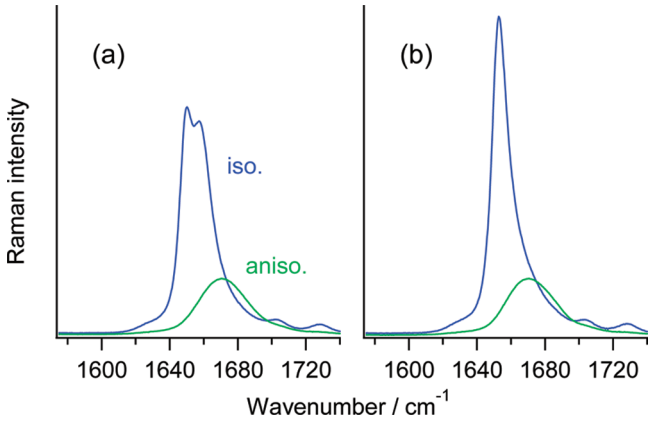

Figure 7. C═O stretching isotropic and anisotropic Raman band profiles of liquid DMF normal/d_6 equimolar mixture (a) synthesized as simple addition of the observed band profiles of the two neat liquids, and (b) measured for the real mixture. No dilution effect (shifts) on the frequencies of the component bands has been included for the former.

of the DMF normal/^{13}C═O mixtures is concerned, we recognize that its distribution between the two bands in the isotropic Raman spectrum is far from being proportional to the corresponding mixture concentration, although the bands of the two neat liquids have almost the same intensities. This is particularly evident in the isotropic Raman spectrum of the equimolar mixture, whereas the intensity distribution of the two bands in the anisotropic Raman spectrum is approximately the same. This intensity bias is a further manifestation of intermolecular vibrational coupling,[52] as will be commented below in connection with the analysis of the calculated spectra of DMF normal/^{13}C═O mixtures.

A rather different situation is encountered in the second case, that of the normal/d_6 mixtures, in both the isotropic and anisotropic Raman spectra. Here, instead of two distinct C═O stretching bands, one for each mixture component, only one band appears in the isotropic Raman spectrum with a frequency (first moment) moving from that of the neat normal species (1662 cm^{-1}) to that of the neat d_6 species (1651 cm^{-1}) upon dilution, as shown in Figure 6b. The same holds with approximately the same rate of frequency change in the anisotropic Raman spectrum, which moves from that of the neat normal species (1677 cm^{-1}) to that of the neat d_6 species (1668 cm^{-1}). This behavior, referred to as "merged-band behavior", was previously observed for the C═O stretching band of formamide in the HCOND$_2$/DCOND$_2$ isotopic liquid mixtures,[51] where the C═O stretching bands of the two species appeared to merge into one band with a frequency moving from that of one neat liquid to the other (1640 cm^{-1} for HCOND$_2$ and 1617 cm^{-1} for DCOND$_2$) upon dilution. In that case, this band merger is not arising from a simple overlap of the bands of the two species, and the possibility of the occurrence of rapid H−D exchange is excluded from chemical considerations. In the case of the liquid DMF normal/d_6 mixtures also, we can exclude the possibility of the band collapsing effects due to rapid H−D exchange for the same reasons, and we can also exclude the possibility that the band is a simple overlap of those of the two species separated by 9 cm^{-1} in the neat liquids, as shown in Figure 7, where the isotropic Raman band profile synthesized by simply adding the bands of the two neat liquids is compared with that of the real liquid mixture.

In interpreting the dilution behavior observed for the normal/d_1 mixtures, the presence of non-negligible satellite bands mentioned in section 2C should be taken into account. In the isotropic Raman spectrum of the neat d_1 species, there is a weak band at 1680 cm^{-1} (as shown in the lowest part in Figure 3a), which is probably arising from the overtone state $2\nu_{16}$ of this species (where ν_{16} is the N−CH$_3$ stretching mode[63]). With decreasing concentration of the d_1 species, this overtone band should progressively decrease in intensity and eventually disappear. However, at x_{normal} = 0.50 a component of noticeable intensity appears at 1669 cm^{-1}, which is considered to be the C═O stretching band of the normal species upshifted by dilution. This 1669 cm^{-1} band is significantly weaker than the 1643.5 cm^{-1} band of the d_1 species, indicating that there is a considerable intensity bias, similarly to (but more significantly than) the case of the normal/^{13}C═O mixtures.

If we now turn to panels c and d of Figures 3−5, we realize that the isotropic and anisotropic Raman spectra of the C═O stretching oscillators in the different isotopic mixtures, calculated according to eq 6, very closely reproduce the corresponding experimental ones shown in panels a and b. Note that only the C═O stretching oscillators are taken into account in these calculations as explained in section 3B, so that no satellite bands are reproduced. Specifically, they unambiguously confirm the following main observed findings. (1) The separate-band behavior is seen in the isotropic Raman spectra of the normal/^{13}C═O mixtures, with a remarkable frequency shift and intensity bias (Figure 5). In the anisotropic Raman spectrum, the bands of both species remain at approximately the same frequencies without noticeable intensity bias. It has been shown[52] that this different behavior in the two spectra is another consequence of the intermolecular vibrational coupling, giving rise to a more remarkable effect on the isotropic Raman spectrum (originating only from the in-phase mode) than on the anisotropic one (with significant contributions from the out-of-phase modes). (2) The merged-band behavior is seen in the isotropic and anisotropic Raman spectra of the normal/d_6 mixtures, with the frequency of the merged band moving from that of the neat normal species to that of the neat d_6 species upon dilution (Figure 4). (3) We regard the spectral behavior shown by the isotropic Raman spectra of the normal/d_1 mixtures (Figure 3) as an intermediate case between

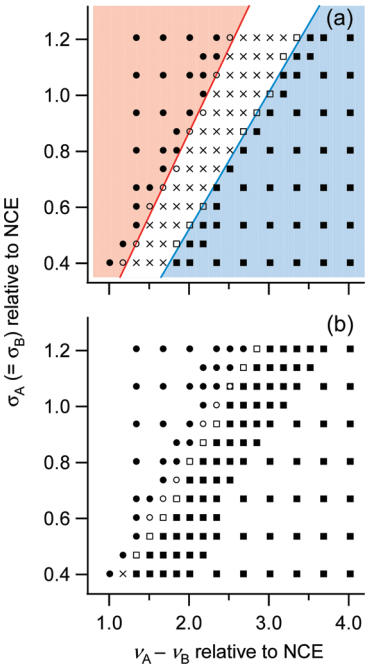

Figure 8. Map of the merged-/separate-band profiles calculated for the (a) isotropic Raman and (b) anisotropic Raman bands of equimolar mixture model liquids,[52] as a function of the frequency separation between the two species relative to the NCE [$(\nu_A - \nu_B)$/NCE] and the standard deviations of the intensity distributions relative to the NCE [σ_A $(=\sigma_B)$/NCE]. Filled squares, separate band profile; filled circles, merged band profile; crosses, band profile with a clear shoulder, characterized by the presence of two extra inflection points but without sign inversion of the gradient on one side of the main band; open squares and circles, judged as on the boundary. In (a) the zones of the merged-/separate-band profiles of the isotropic Raman band are marked with red and blue, respectively.

the separate-band and the merged-band behavior. Here, the band of the normal species is clearly seen at $x_{normal} = 0.75$ but with a weaker intensity than that of the d_1 species in spite of the 3:1 ratio of the mole fractions, only slightly seen at $x_{normal} = 0.50$, and negligibly seen at $x_{normal} = 0.25$. In the anisotropic Raman spectra, such effects cannot be seen.

In the light of the good agreement between the calculated and observed isotropic and anisotropic Raman spectra, we can assert that the time-domain calculations performed in the present study incorporate all the fundamental physical aspects controlling the main features of the spectral intensity distributions (i.e., the band frequency shifts, the NCE, and the merged-/separate-band behavior) of the C═O stretching bands in these mixtures. The important factors are the dynamically modulated environment perturbation (eq 1) and the resonant (and nearly resonant) intermolecular vibrational coupling between the C═O stretching oscillators based on the TDC mechanism (eq 3). As the resonance condition between the oscillators present in the mixture becomes progressively closer (from normal/^{13}C═O, normal/d_1, to normal/d_6), the TDC between oscillators becomes more effective and, eventually, makes them oscillate with the same frequency. Therefore, the merged-/separate-band behavior of nearly resonant oscillators is controlled by the same type of term of the vibrational Hamiltonian that gives rise to the NCE.

To support consideration on how the properties of the C═O stretching oscillators of the two species [their frequencies ν_A and ν_B and bandwidths (standard deviations) σ_A and σ_B] affect the observed spectral profiles with regard to the merged-/separate-band behavior in the presence of intermolecular vibrational coupling, we refer to the results of the isotropic and anisotropic Raman intensity distributions calculated for the equimolar model liquid mixtures with various parameters of oscillator properties.[52] The results are shown in Figure 8 in the form of a map of the calculated band profiles plotted against the reduced quantities, $(\nu_A - \nu_B)$/NCE (frequency separation between the two species relative to the NCE) and σ_A (assumed as equal to σ_B)/NCE (standard deviations of the intensity distributions relative to the NCE). In Figure 8a three different zones can be recognized in the map for the isotropic Raman spectra: the zone on the left-hand side (marked in red) representing the region where the merged-band behavior is seen, the zone on the right-hand side (marked in blue) where the separate-band behavior is seen, and the zone in between where the intermediate behavior is seen. In the map for the anisotropic Raman spectra shown in Figure 8b, the third zone is essentially absent. The behavior (separate, merged, and intermediate) of the isotropic Raman spectra found for the liquid DMF isotopic mixtures in the present study can be retrieved on the map shown in Figure 8a, at [$(\nu_A - \nu_B)$/NCE, σ_A $(=\sigma_B)$/NCE] = (2.5, 0.4) in the separate-band zone for the normal/^{13}C═O mixtures, at (0.4, 0.4) (out of the range of this map) in the merged-band zone for the normal/d_6 mixtures, and at (1.1, 0.4) on a boundary of the zones for the normal/d_1 mixtures. It should be noted that the maps shown in Figure 8 are formulated with NCE-reduced parameters, and thus offer more general applicability than those displayed in ref 52. In fact, the latter were drawn with a fixed value of the dipole derivative (3.397 D Å^{-1} amu$^{-1/2}$), while the NCE-reduced parameters employed for the former are essentially scaled with the square of the dipole derivative (because NCE is proportional to it$^{1-3}$) and are therefore applicable to oscillators with any value of dipole derivative.

B. Calculated 1D- and 2D-IR Spectra. Based on the result in section 4A indicating that the time-domain computational procedure adopted in the present study incorporates all the fundamental physical aspects controlling the main spectral features, we have calculated the 1D- and 2D-IR spectra as theoretical predictions to see how the effect of nearly resonant intermolecular vibrational coupling between different species is seen in the profiles of those spectra. Since it turns out that the most interesting spectral features (as an intermediate case) are seen for the normal/d_1 mixture as remarked in section 4A, our discussion is concentrated on this mixture and the related neat liquids.

The spectra calculated for the neat normal species, neat d_1 species, and their 1:1 mixture are shown in Figure 9. For comparison, the spectra obtained by simply adding those of two neat liquids are also shown. (The additions are done for amplitudes and not for absolute values themselves plotted in Figure 9e,j,o,t.)

For the absorptive 2D-IR spectra of two neat liquids (Figure 9c,h), it is recognized that the nodal line separating the positive and negative bands is tilted at around the peak frequency (its position being indicated by the vertical dotted line in each spectrum). Generally, this tilt may originate from the inhomogeneous band broadening.[78,79] However, in the case of the C═O stretching band of liquid DMF, the frequency modulations are sufficiently rapid, so that the nodal line becomes essentially horizontal if the resonant intermolecular vibrational coupling is switched off.[60] Therefore, in this case, the tilt originates almost totally from the intermolecular vibrational coupling. Another feature of the absorptive 2D-IR spectra arising from the intermolecular vibrational

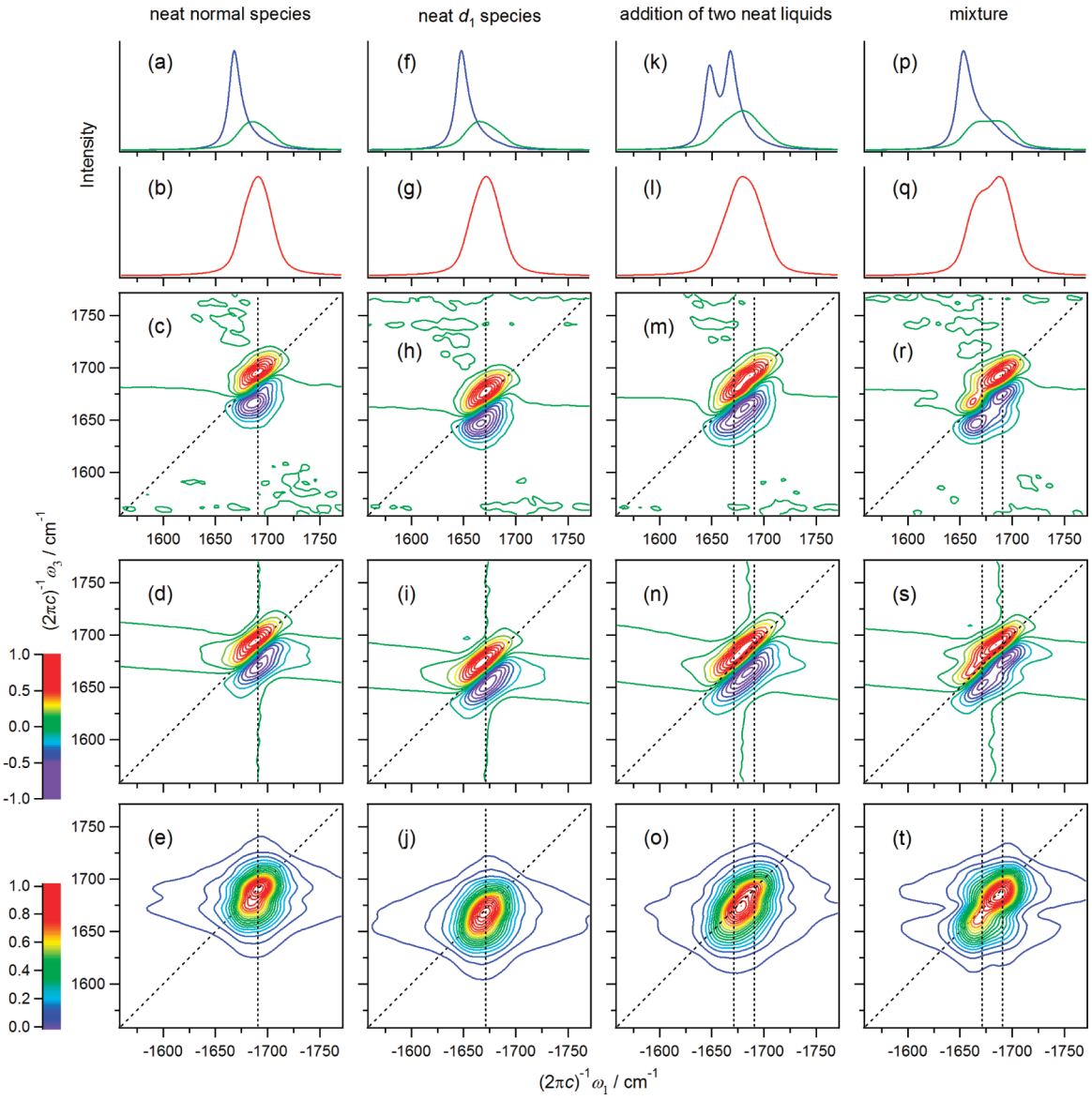

Figure 9. 1D-IR and Raman, and 2D-IR spectra calculated for neat liquid DMF normal and d_1 species and their 1:1 mixture in the C═O stretching mode spectral region. The spectra synthesized by simply adding those of the two neat liquids are also shown for comparison. Each spectrum is shown in a separate relative intensity scale. (a,f,k,p) Isotropic (blue) and anisotropic (green) Raman spectra; (b,g,l,q) IR spectra; (c,h,m,r) absorptive 2D-IR spectra, real part; (d,i,n,s) rephasing 2D-IR spectra, real part; (e,j,o,t) rephasing 2D-IR spectra, absolute value signals. The 2D-IR spectra are calculated with the *zzzz* polarization. The vertical dotted lines in the 2D-IR spectra indicate the peak positions of the calculated 1D-IR spectra of neat liquids.

coupling is that the peak intensity of the negative band is somewhat smaller than that of the positive band.[60]

The absorptive 2D-IR spectrum of the normal/d_1 1:1 mixture (Figure 9r) might look as if it simply consisted of the bands of the two neat liquids. However, comparing with the spectrum synthesized as a simple addition of those of the two neat liquids (Figure 9m), it can be recognized that a band splitting occurs with a significant intensity bias (especially for the positive band) in the mixture because of the vibrational coupling between the molecules of the two different species. The splitting is also seen in the 1D-IR and anisotropic Raman spectra (Figure 9p,q), but it is more clearly seen in the absorptive 2D-IR spectrum. It is considered to be natural that the vibrational bands of the coupled modes are split to some extent. In this sense, the merger of the bands observed and calculated for the isotropic Raman spectrum discussed in section 4A is rather remarkable. The intensity bias in the 1D- and 2D-IR spectra occurs to the high-frequency side, in contrast to the isotropic Raman spectrum (Figure 3a,c) where it occurs to the low-frequency side. This is related to the difference in the nature (vibrational phase relationship) of the vibrational modes with strong IR intensities from those with strong isotropic Raman intensities. Another characteristic in the absorptive 2D-IR spectrum arising from the vibrational coupling between the two species is the existence of the off-diagonal features located at around $(2\pi c)^{-1}(\omega_1,\omega_3)$ = (1670,1690) and (1690,1655) cm^{-1}. These are not isolated peaks and appear only as flexions of the contour lines, but their existence is recognizable from the comparison with the synthesized simply added spectrum. Similar features (band splitting, intensity bias, and off-diagonal bands) are also seen in the rephasing real part and absolute value spectra shown in Figure 9s,t.

dx.doi.org/10.1021/jp209119e |*J. Phys. Chem. B* 2012, 116, 353–366

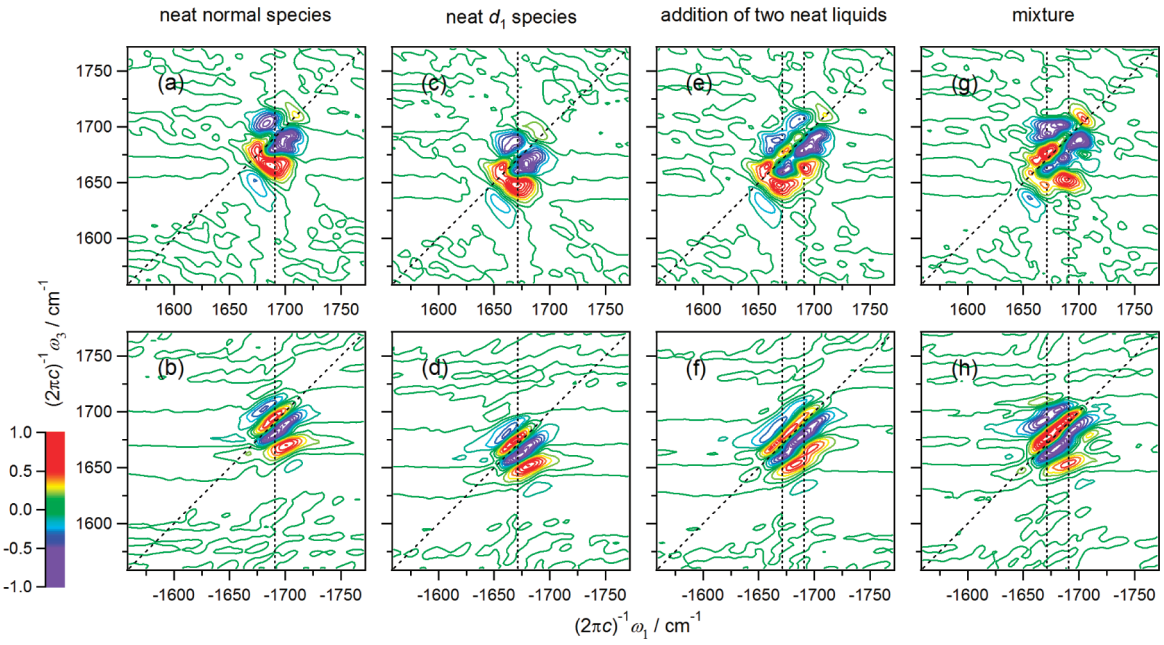

Figure 10. Difference 2D-IR spectra, calculated as $S_{zzzz} - 3S_{xxzz}$, for neat liquid DMF normal and d_1 species and their 1:1 mixture in the C═O stretching mode spectral region. The spectra synthesized by simply adding those of the two neat liquids are also shown for comparison. (a,c,e,g) Absorptive 2D-IR spectra, real part; (b,d,f,h) rephasing 2D-IR spectra, real part. Each spectrum is shown in a separate relative intensity scale. The vertical dotted lines indicate the peak positions of the 1D-IR spectra of neat liquids.

To see more clearly the off-diagonal features, the difference 2D-IR spectra between those of the parallel and perpendicular polarizations ($S_{zzzz} - 3S_{xxzz}$) are calculated. The results are shown in Figure 10. The spectral profiles are not simple even for the neat liquids because of the intermolecular vibrational coupling (between the molecules of the same species). However, the off-diagonal features arising from the vibrational coupling between the two different species are recognized in the spectra of the mixture. In the absorptive 2D-IR spectrum (Figure 10g), clear off-diagonal bands appear at around $(2\pi c)^{-1}(\omega_1,\omega_3) = (1670,1700)$ and $(1690,1650)$ cm^{-1}. These are absent in the synthesized simply added spectrum (Figure 10e), so that they originate from the vibrational coupling between the two different species. In the rephasing 2D-IR spectrum (Figure 10h), the intensity of the off-diagonal feature is somewhat enhanced at around $(2\pi c)^{-1}(\omega_1,\omega_3) = (1670,1700)$ cm^{-1}. This intensity enhancement is recognizable from the comparison with the synthesized simply added spectrum (Figure 10f).

These results clearly indicate that the effect of nearly resonant intermolecular vibrational coupling between different species is sufficiently noticeable in the 2D-IR spectral profiles. It does not seem to be as remarkable as the band merger observed and calculated for the isotropic Raman spectra, but the effect is more clearly seen in the 2D-IR spectra than in the 1D-IR spectra because they are developed along two frequency axes and also because one may use different polarization conditions. Considering from the other side, it is also suggested that the effect of nearly resonant intermolecular vibrational coupling between different species should be taken into account in interpreting 2D-IR spectral profiles.

5. SUMMARY

In the present study, the polarized (isotropic and anisotropic) Raman spectra are measured in the spectral region of the C═O stretching (amide I) band for three types of binary isotopic liquid mixtures of DMF (normal/d_1, normal/d_6, and normal/^{13}C═O) with mole fractions of x_{normal} = 1.00, 0.75, 0.50, 0.25, and 0.00, and are analyzed with the help of theoretical calculations based on a time-domain computational method. Two distinct types of spectral behavior have been found for the isotropic Raman spectra. One is the separate-band behavior, observed and calculated for the normal/^{13}C═O mixtures (Figure 5a,c), where two separate bands (one for each species) appear at all concentrations but with significant intensity bias. For example, in the case of the 1:1 mixture, the band of the normal species is significantly weaker than that of the ^{13}C═O species, although the bands of the two neat liquids have almost the same intensities. The concentration dependence of the frequency positions is linear, as show in Figure 6a. The other is the merged-band behavior, observed and calculated for the normal/d_6 mixtures (Figure 4a,c), where only one band appears with a frequency moving, upon dilution, from that of the neat normal species to that of the neat d_6 species (Figure 6b). This merged band is not a simple overlap of those of the two species, as clearly shown in Figure 7. The spectral behavior observed and calculated for the normal/d_1 mixtures (Figure 3a,c) is regarded as an intermediate case between these two, also with significant intensity bias. In contrast, this intensity bias cannot be seen for all the mixtures in the anisotropic Raman spectra.

All the main spectral features observed for these mixtures (except for the presence of satellite bands) have been well reproduced by the calculations, meaning that the calculations incorporate all the fundamental physical aspects controlling the main spectral features. The important factors are the dynamically modulated environment perturbation (eq 1) and the resonant (and nearly resonant) intermolecular vibrational coupling between the C═O stretching oscillators based on the TDC mechanism (eq 3). It has also been confirmed that the band merger observed for the normal/d_6 mixtures and the intensity bias

observed for the normal/$^{13}C{=}O$ and normal/d_1 mixtures are both controlled by the same type of term (resonant intermolecular vibrational coupling) of the vibrational Hamiltonian that gives rise to the NCE.

Based on this result, the 1D- and 2D-IR spectra of the normal/d_1 1:1 mixture have been calculated as theoretical predictions. An eigenstate-free method as described in section 3D has been employed to increase the efficiency of the calculations and, hence, to do calculations on a largest possible system. It has been found that a band splitting occurs with a significant intensity bias in the 1D- and 2D-IR spectra (more noticeably in the latter, as seen in Figure 9), and this intensity bias is to the opposite side from that observed in the isotropic Raman spectrum. Some off-diagonal features are also seen in the 2D-IR spectra. These spectral features arise from the nearly resonant vibrational coupling between the two species. In other words, the effect of nearly resonant intermolecular vibrational coupling between different species should be taken into account in interpreting 2D-IR spectral profiles.

Summarizing these results, it has been shown that there are varieties of spectroscopic phenomena arising from resonant (and nearly resonant) intermolecular vibrational coupling. Since this coupling is reasonably represented by a physical mechanism (TDC), this situation is expected to occur in any cases where oscillators with sufficiently large dipole derivatives and sufficiently similar vibrational frequencies are spatially located close to each other. In fact, the isotopic substitution technique is widely used to effectively decouple a particular vibration from the others in the presence of strong intermolecular (or interpeptide) vibrational interactions, for the purpose of simplification of the interpretation of the spectral profiles. For example, in the case of the OH stretch, the H/D substitution is surely useful for this purpose, because of the very large frequency separation between the OH stretch and the OD stretch. However, in many other cases of isotopic substitution, e.g., in the case of the amide I mode of the peptide groups in proteins upon $^{12}C{=}O/^{13}C{=}O$ substitution, a nearly resonant situation is considered to occur, because the frequency separation is not so large. The vibrational decoupling is often judged on the basis only of the frequency positions, but the intensity distribution is also an important factor that constitutes the vibrational band profiles. The results of the present study indicate that insight into the structures of those systems will be provided by analyzing the spectral features, preferably of both the IR and Raman spectra, especially with regard not only to the frequency positions but also to the intensity distributions.

AUTHOR INFORMATION

Corresponding Author

*E-mail: torii@ed.shizuoka.ac.jp (H.T.); mariagrazia.giorgini@unibo.it (M.G.G.).

ACKNOWLEDGMENT

The theoretical part of this study was supported by a Grant-in-Aid for Scientific Research from the Ministry of Education, Culture, Sports, Science, and Technology of Japan provided to H.T.

REFERENCES

(1) Torii, H. In *Novel Approaches to the Structure and Dynamics of Liquids: Experiments, Theories and Simulations*; Samios, J., Durov, V. A., Eds.; Kluwer: Dordrecht, The Netherlands, 2004; pp 343−360.
(2) Logan, D. E. *Chem. Phys.* **1986**, *103*, 215–225.
(3) Torii, H.; Tasumi, M. *J. Chem. Phys.* **1993**, *99*, 8459–8465.
(4) Krimm, S.; Abe, Y. *Proc. Natl. Acad. Sci. U.S.A.* **1972**, *69*, 2788–2792.
(5) Torii, H.; Tasumi, M. *J. Chem. Phys.* **1992**, *96*, 3379–3387.
(6) Murphy, W. F.; Bernstein, H. J. *J. Phys. Chem.* **1972**, *76*, 1147–1152.
(7) Scherer, J. R.; Go, M. K.; Kint, S. *J. Phys. Chem.* **1974**, *78*, 1304–1313.
(8) Walrafen, G. E. *J. Chem. Phys.* **2005**, *122*, 174502.
(9) Buch, V. *J. Phys. Chem. B* **2005**, *109*, 17771–17774.
(10) Torii, H. *J. Phys. Chem. A* **2006**, *110*, 9469–9477.
(11) Torii, H. *J. Mol. Liq.* **2007**, *136*, 274–280.
(12) Auer, B. M.; Skinner, J. L. *J. Chem. Phys.* **2008**, *128*, 224511.
(13) Yang, M.; Skinner, J. L. *Phys. Chem. Chem. Phys.* **2010**, *12*, 982–991.
(14) Torii, H. *J. Phys. Chem. B* **2010**, *114*, 13403–13409.
(15) Perchard, C.; Perchard, J. P. *J. Raman Spectrosc.* **1975**, *3*, 277–302.
(16) Torii, H. *J. Phys. Chem. A* **1999**, *103*, 2843–2850.
(17) Musso, M.; Torii, H.; Ottaviani, P.; Asenbaum, A.; Giorgini, M. G. *J. Phys. Chem. A* **2002**, *106*, 10152–10161.
(18) Zheng, R.; Sun, Y.; Shi., Q. *Phys. Chem. Chem. Phys.* **2011**, *13*, 2027–2035.
(19) Schindler, W.; Sharko, P. T.; Jonas, J. *J. Chem. Phys.* **1982**, *76*, 3493–3496.
(20) Giorgini, M. G.; Fini, G.; Mirone, P. *J. Chem. Phys.* **1983**, *79*, 639–643.
(21) Musso, M.; Giorgini, M. G.; Döge, G.; Asenbaum, A. *Mol. Phys.* **1997**, *92*, 97–104.
(22) Bertie, J. E.; Michaelian, K. H. *J. Chem. Phys.* **1998**, *109*, 6764–6771.
(23) Torii, H.; Musso, M.; Giorgini, M. G.; Asenbaum, A.; Döge, G. *Mol. Phys.* **1998**, *98*, 821–828.
(24) Musso, M.; Torii, H.; Giorgini, M. G.; Döge, G. *J. Chem. Phys.* **1999**, *110*, 10076–10085.
(25) Giorgini, M. G.; Musso, M.; Torii, H. *J. Phys. Chem. A* **2005**, *109*, 5846–5854.
(26) Torii, H.; Musso, M.; Giorgini, M. G. *J. Phys. Chem. A* **2005**, *109*, 7797–7804.
(27) Musso, M.; Giorgini, M. G.; Torii, H.; Dorka, R.; Asenbaum, A.; Keutel, D.; Oehme, K.-L. *J. Mol. Liq.* **2006**, *125*, 115–122.
(28) Torii, H.; Tasumi, M. *J. Raman Spectrosc.* **1998**, *29*, 81–86.
(29) Schweitzer-Stenner, R. *J. Raman Spectrosc.* **2001**, *32*, 711–732.
(30) Cha, S.; Ham, S.; Cho, M. *J. Chem. Phys.* **2002**, *117*, 740–750.
(31) Brauner, J. W.; Flach, C. R.; Mendelsohn, R. *J. Am. Chem. Soc.* **2005**, *127*, 100–109.
(32) Kim, J.; Huang, R.; Kubelka, J.; Bouř, P.; Keiderling, T. A. *J. Phys. Chem. B* **2006**, *110*, 23590–23602.
(33) Gorbunov, R. D.; Stock, G. *Chem. Phys. Lett.* **2007**, *437*, 272–276.
(34) Jansen, T. l. C.; Knoester, J. *J. Phys. Chem. B* **2006**, *110*, 22910–22916.
(35) Torii, H. *J. Phys. Chem. B* **2007**, *111*, 5434–5444.
(36) Torii, H. *Mol. Phys.* **2009**, *107*, 1855–1866.
(37) Piryatinski, A.; Tretiak, S.; Chernyak, V.; Mukamel, S. *J. Raman Spectrosc.* **2000**, *31*, 125–135.
(38) Watson, T. M.; Hirst, J. D. *J. Phys. Chem. A* **2003**, *107*, 6843–6849.
(39) Eker, F.; Griebenow, K.; Cao, X.; Nafie, L. A.; Schweitzer-Stenner, R. *Biochemistry* **2004**, *43*, 613–621.
(40) Mikhonin, A. V.; Asher, S. A. *J. Phys. Chem. B* **2005**, *109*, 3047–3052.
(41) Karjalainen, E. L.; Ravi, H. K.; Barth, A. *J. Phys. Chem. B* **2011**, *115*, 749–757.
(42) Volkov, V. V.; Chelli, R.; Muniz-Miranda, F.; Righini., R. *J. Phys. Chem. B* **2011**, *115*, 5294–5303.
(43) Fini, G.; Mirone, P.; Fortunato, B. *J. Chem. Soc., Faraday Trans. 2* **1973**, *69*, 1243–1248.

(44) Mirone, P.; Fini, G. *J. Chem. Phys.* **1979**, *71*, 2241–2243.
(45) Woutersen, S.; Bakker, H. J. *Nature* **1999**, *402*, 507–509.
(46) Cowan, M. L.; Bruner, B. D.; Huse, N.; Dwyer, J. R.; Chugh, B.; Nibbering, E. T. J.; Elsaesser, T.; Miller, R. J. D. *Nature* **2005**, *434*, 199–202.
(47) Yagasaki, T.; Ono, J.; Saito, S. *J. Chem. Phys.* **2009**, *131*, 164511.
(48) Paarmann, A.; Hayashi, T.; Mukamel, S.; Miller, R. J. D. *J. Chem. Phys.* **2008**, *128*, 191103.
(49) Paarmann, A.; Hayashi, T.; Mukamel, S.; Miller, R. J. D. *J. Chem. Phys.* **2009**, *130*, 204110.
(50) Jansen, T. l. C.; Auer, B. M.; Yang, M.; Skinner, J. L. *J. Chem. Phys.* **2010**, *132*, 224503.
(51) Mortensen, A.; Nielsen, O.-F.; Yarwood, J.; Shelley, V. *J. Phys. Chem.* **1995**, *99*, 4435–4440.
(52) Torii, H.; Osada, Y.; Iwami, M. *J. Raman Spectrosc.* **2008**, *39*, 1592–1599.
(53) Hamm, P.; Lim, M.; DeGrado, W. F.; Hochstrasser, R. M. *Proc. Natl. Acad. Sci. U.S.A.* **1999**, *96*, 2036–2041.
(54) Asplund, M. C.; Lim, M.; Hochstrasser, R. M. *Chem. Phys. Lett.* **2000**, *323*, 269–277.
(55) Zhao, W.; Wright, J. C. *Phys. Rev. Lett.* **2000**, *84*, 1411–1414.
(56) Chung, H. S.; Khalil, M.; Tokmakoff, A. *J. Phys. Chem. B* **2004**, *108*, 15332–15342.
(57) Moran, A. M.; Park, S.-M.; Mukamel, S. *J. Chem. Phys.* **2003**, *118*, 9971–9980.
(58) Ishizaki, A.; Tanimura., Y. *J. Phys. Chem. A* **2007**, *111*, 9269–9276.
(59) Torii, H. *Chem. Phys. Lett.* **2005**, *414*, 417–422.
(60) Torii, H. *J. Phys. Chem. A* **2006**, *110*, 4822–4832.
(61) Torii, H. *Vib. Spectrosc.* **2006**, *42*, 140–146.
(62) Torii, H. *J. Phys. Chem. A* **2002**, *106*, 3281–3286.
(63) Jao, T. C.; Scott, I.; Steele, D. *J. Mol. Spectrosc.* **1982**, *92*, 1–17.
(64) Note that the frequency of this component is different from that of the neat liquid $^{13}C{=}O$ species because of the presence of the resonant intermolecular vibrational coupling in the latter. For the spectra of the d_1 and d_6 species, this component d is regarded as arising from $D^{13}CON(CH_3)_2$ and $H^{13}CON(CD_3)_2$, respectively, contained also as natural impurity.
(65) Jorgensen, W. L.; Swenson, C. J. *J. Am. Chem. Soc.* **1985**, *107*, 569–578.
(66) Ham, S.; Kim, J. H.; Lee, H.; Cho, M. *J. Chem. Phys.* **2003**, *118*, 3491–3498.
(67) Torii, H. *J. Chem. Phys.* **2003**, *119*, 2192–2198.
(68) Bouř, P.; Keiderling, T. A. *J. Chem. Phys.* **2003**, *119*, 11253–11262.
(69) Fecko, C. J.; Eaves, J. D.; Loparo, J. J.; Tokmakoff, A.; Geissler, P. L. *Science* **2003**, *301*, 1698–1702.
(70) Corcelli, S. A.; Lawrence, C. P.; Skinner, J. L. *J. Chem. Phys.* **2004**, *120*, 8107–8117.
(71) Hayashi, T.; Hamaguchi, H. *Chem. Phys. Lett.* **2000**, *326*, 115–122.
(72) Hayashi, T.; Jansen, T. l. C.; Zhuang, W.; Mukamel, S. *J. Phys. Chem. A* **2005**, *109*, 64–82.
(73) Steele, D.; Quatermain, A. *Spectrochim. Acta* **1987**, *43A*, 781–789.
(74) Frisch, M. J.; Trucks, G. W.; Schlegel, H. B.; Scuseria, G. E.; Robb, M. A.; Cheeseman, J. R.; Montgomery, J. A., Jr.; Vreven, T.; Kudin, K. N.; Burant, J. C. et al. *Gaussian 03, Revision D.01*; Gaussian, Inc.: Wallingford, CT, 2004.
(75) Giorgini, M. G.; Musso, M.; Asenbaum, A.; Döge, G. *Mol. Phys.* **2000**, *98*, 783–791.
(76) Shelley, V.; Yarwood, J. *Chem. Phys.* **1989**, *137*, 277–280.
(77) Knapp, E. W.; Fischer, S. F. *J. Chem. Phys.* **1982**, *76*, 4730–4735.
(78) Fang, C.; Hochstrasser, R. M. *J. Phys. Chem. B* **2005**, *109*, 18652–18663.
(79) Wang, J.; Chen, J.; Hochstrasser, R. M. *J. Phys. Chem. B* **2006**, *110*, 7545–7555.